Lawrence Berkeley National Laboratory
Recent Work

Title
SILICON DEPOSITION ON A ROTATING DISK

Permalink
https://escholarship.org/uc/item/3h084033

Author
Pollard, R.

Publication Date
1979-05-01

eScholarship.org Powered by the California Digital Library
University of California

LBL-9154 c.1
Preprint

Lawrence Berkeley Laboratory
UNIVERSITY OF CALIFORNIA

Materials & Molecular Research Division

Submitted to the Journal of the Electrochemical Society

SILICON DEPOSITION ON A ROTATING DISK

Richard Pollard and John Newman

May 1979

RECEIVED
LAWRENCE
BERKELEY LABORATORY
OCT 15 1979
LIBRARY AND
DOCUMENTS SECTION

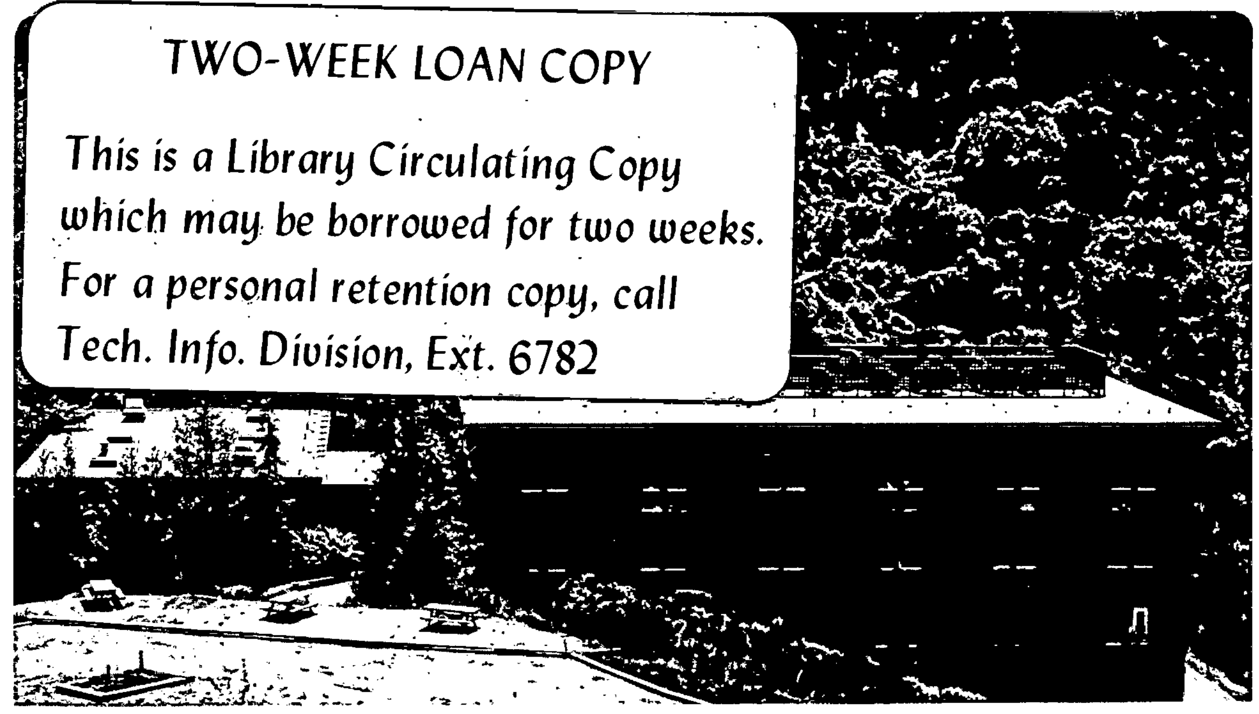

LBL-9154 c.1

Prepared for the U. S. Department of Energy
under Contract W-7405-ENG-48

DISCLAIMER

This document was prepared as an account of work sponsored by the United States Government. While this document is believed to contain correct information, neither the United States Government nor any agency thereof, nor the Regents of the University of California, nor any of their employees, makes any warranty, express or implied, or assumes any legal responsibility for the accuracy, completeness, or usefulness of any information, apparatus, product, or process disclosed, or represents that its use would not infringe privately owned rights. Reference herein to any specific commercial product, process, or service by its trade name, trademark, manufacturer, or otherwise, does not necessarily constitute or imply its endorsement, recommendation, or favoring by the United States Government or any agency thereof, or the Regents of the University of California. The views and opinions of authors expressed herein do not necessarily state or reflect those of the United States Government or any agency thereof or the Regents of the University of California.

LBL-9154

Silicon Deposition on a Rotating Disk

Richard Pollard and John Newman

Materials and Molecular Research Division, Lawrence Berkeley Laboratory
and Department of Chemical Engineering, University of California,
Berkeley, California 94720

May 1979

ABSTRACT

A one-dimensional model has been developed which describes the interactions between hydrodynamics, multicomponent heat and mass transfer, and reaction kinetics for the rotating disk system. The analysis includes variable physical properties and finite interfacial velocity and has provision for an arbitrary number of simultaneous homogeneous and heterogeneous reactions. The model has been applied to the chemical vapour deposition of silicon from silicon tetrachloride in excess hydrogen. Predictions for the dependence of silicon production rate on disk temperature and rotation rate are compared with available experimental data.

INTRODUCTION

Many chemical syntheses with important industrial applications involve simultaneous homogeneous and heterogeneous reactions. In the semiconductor industry there is considerable interest in chemical vapour deposition of high quality silicon and germanium. Tubular reactors, where reactant gases pass across the growing surface, have been used for silicon deposition from $SiCl_4$ (alternatively, $SiHCl_3$ or $SiCl_2$) in excess hydrogen. Experimental studies in these systems have included spectroscopic identification of gas phase species and measurement of composition, temperature, and velocity profiles in the diffusion layer adjacent to the susceptor surface [1-4].

A theoretical analysis of silicon deposition in a tubular flow reactor has considered the effects of heat, mass, and momentum transfer [5]. However, the complex nature of the transport processes necessitated incorporation of certain assumptions, such as constant physical properties and fully developed flow profiles, into the model.

The rotating disk has been used to study chemical vapour deposition because the hydrodynamics and mass transfer characteristics of this system are relatively well understood. A one-dimensional model has been developed for the transport-limited reaction of iodine and germanium [6]. This analysis includes the effects of density variations in the boundary layer, multicomponent diffusion, and finite interfacial velocity. However, it is assumed that the system is isothermal and that the axial velocity depends linearly on the distance from the disk surface. Epitaxial growth

of silicon has also been studied by the rotating disk method [7]. The model includes natural convection and temperature variations but it assumes constant physical properties and equilibrium in the gas phase, and it is not able to account fully for the experimentally observed temperature dependence of silicon growth rate.

This paper presents a general approach to the analysis of silicon deposition on a rotating disk. The model considers multicomponent heat and mass transfer, coupled with laminar fluid flow, and simultaneous homogeneous and heterogeneous reactions with finite reaction rates. Variable physical properties are included, as well as a finite interfacial velocity at the disk surface. The analysis can be used to investigate the influence of disk temperature and rotation rate on the deposition process and to consider the rate-limiting factors in the system. The formulation of the silicon deposition problem has been developed in a general manner so that it can be readily applied to a wide variety of different physical situations.

Transport Phenomena

Momentum, heat and mass transfer for a rotating disk are modelled subject to the following restrictions: (1) steady-state operation; (ii) laminar flow of Newtonian fluid; (iii) no viscous dissipation of energy; (iv) radiation and natural convection neglected; (v) no end effects; (vi) ideal gas mixture. These assumptions simplify the calculational procedure significantly. The ideal gas condition is necessary in the absence of information required to justify a more sophisticated equation of state. The validity of assumptions (iv) and (v) is discussed below.

With these restrictions, it can be shown that the velocity component normal to the disk, and the gas composition, depend only on the axial coördinate, so that the surface is uniformly accessible from a mass transfer standpoint. Consequently, the transport properties are also independent of radial position, and the problem becomes one-dimensional.

The transformation of von Kármán [8] suggests that, with cylindrical coördinates, the velocity components and the pressure can be expressed as [9]:

$$\left.\begin{aligned} v_r = r\,\Omega\,F(\zeta)\,, \quad v_\theta = r\,\Omega\,G(\zeta)\,, \quad v_z = \sqrt{\nu_\infty \Omega}\,H(\zeta) \\ p = \mu_\infty\,\Omega P\,(\zeta) + g_z \int_0^z \rho dz \end{aligned}\right\} \tag{1}$$

where

$$\zeta = z\,\sqrt{\Omega/\nu_\infty} \tag{2}$$

and where the direction of gravitational acceleration is taken to be perpendicular to the disk surface. Equations (1) define dimensionless functions F, G, H, and P and show how velocity components and pressure depend on disk rotation speed and on the coördinates for radial and axial position, r and ζ.

The steady-state equations of motion and continuity of the fluid are:

$$\rho\,\underline{v}\cdot\nabla\,\underline{v} = -\nabla p - \nabla\cdot\,\underline{\underline{\tau}} + \rho\underline{g} \tag{3}$$

$$\nabla\cdot(\rho\underline{v}) = 0 \tag{4}$$

where the viscous stress for a Newtonian fluid is

$$\underline{\underline{\tau}} = -\mu[\nabla\underline{v} + (\nabla\underline{v})^T] + \frac{2}{3}\,\mu\underline{\underline{I}}\;\nabla\cdot\underline{v} \tag{5}$$

Substitution of Eq. (1) into equations (3) and (4), gives

$$2F + H' = - H \frac{d\ln\rho}{d\zeta} \quad (6)$$

for the continuity equation and, with Eq. (5) ,

$$\left.\begin{aligned} F^2 - G^2 + HF' &= - \frac{\rho_\infty}{\rho} \frac{d}{d\zeta} \left(\frac{\mu F'}{\mu_\infty} \right) \\ 2FG + HG' &= \frac{\rho_\infty}{\rho} \frac{d}{d\zeta} \left(\frac{\mu G'}{\mu_\infty} \right) \end{aligned}\right\} \quad (7)$$

$$\frac{\rho}{\rho_\infty} HH' + P' = \frac{4}{3} \frac{d}{d\zeta} \left[\frac{\mu}{\mu_\infty} (H'-F) \right] + \frac{2\mu F'}{\mu_\infty} \quad (8)$$

for the equations of motion [10]. The boundary conditions include

$$\left.\begin{aligned} F = 0,\ G = 1 \quad &\text{at } \zeta = 0 \\ F = G = 0 \quad &\text{at } \zeta = \infty \ . \end{aligned}\right\} \quad (9)$$

In addition, the normal velocity component is related to the mass transfer rate at the surface by the definition for the mass average velocity,

$$\underline{v} = \frac{1}{\rho} \sum_i M_i \underline{N}_i \quad , \quad (10)$$

where N_i is the molar flux of species i.

The fluid density ρ, used in the equations above, is directly related to total gas concentration by

$$\rho = \bar{M} c \quad , \quad (11)$$

where $\bar{M} = \sum_i x_i M_i$. The concentration is, in turn, related to pressure with the ideal gas law,

$$p = cRT \quad . \quad (12)$$

A steady-state, thermal energy equation for an ideal gas mixture can be rewritten as [11]

$$c\tilde{C}_p \underline{v}\cdot\nabla T = \nabla\cdot(k\nabla T) + \underline{v}\cdot\nabla p - \sum_i (\underline{J}_i\cdot\nabla\bar{H}_i + \bar{H}_i R_i) \quad , \tag{13}$$

provided that viscous energy dissipation and the Dufour energy flux can be neglected. The last term on the right represents thermal effects due to interdiffusion of species and homogeneous chemical reactions, $\underline{J}_i$ is the flux of species i relative to the mass average velocity, given by

$$\underline{J}_i = \underline{N}_i - c_i\underline{v} \quad , \tag{14}$$

and $\tilde{C}_p$ is the mean specific heat of the mixture, defined as

$$\tilde{C}_p = \sum_i x_i\tilde{C}_{pi} \quad . \tag{15}$$

Equation (13) can be expressed in dimensionless form as

$$\frac{\tilde{C}_p}{\tilde{C}_{p\infty}} HT' = \frac{T}{Pr_\infty T_\infty}\left[\frac{k}{k_\infty} T'' + T' \frac{d(k/k_\infty)}{d\zeta}\right] + \frac{RTH}{\tilde{C}_{p\infty}}\frac{d\ln p}{d\zeta} + \frac{sTT'}{T_\infty} + UT \tag{16}$$

The dimensionless quantities Pr_∞, s, and U are defined by

$$Pr_\infty = \frac{p\ \mu_\infty\tilde{C}_{p\infty}}{p_\infty k_\infty \bar{M}_\infty} \quad , \tag{17}$$

$$s = \frac{-p_\infty \sum_i J_i\tilde{C}_{pi}}{p\ \tilde{C}_{p\infty}} \quad , \tag{18}$$

and

$$U = -\frac{P_\infty \sum_i \tilde{H}_i^* \mathcal{R}_i}{p T_\infty \tilde{C}_{p\infty}} \quad , \tag{19}$$

respectively, where $\mathcal{J}_i = \underline{J}_i / c_\infty \sqrt{\nu_\infty \Omega}$, and $\mathcal{R}_i = R_i / c_\infty \Omega$, and where $\bar{H}_i = \tilde{H}_i^*$ for an ideal gas. The temperatures of the disk and the bulk fluid are specified as boundary conditions for Eq. (16).

The multicomponent diffusion equation [11]

$$c_i \left(\nabla \mu_i + \bar{S}_i \nabla T - \frac{M_i \nabla p}{\rho} \right) = RT \sum_{k \neq i} \frac{c_i c_k}{c \mathcal{D}_{ik}} \left[\underline{v}_k - \underline{v}_i + \left(\frac{D_k^T}{\rho_k} - \frac{D_i^T}{\rho_i} \right) \nabla \ln T \right] \tag{20}$$

describes the motion of species i relative to the surrounding fluid. If thermal diffusion is assumed to be negligible, and if the gas mixture behaves ideally, Eq. (20) may be written in dimensionless form as

$$\nabla x_i + x_i \left(1 - \frac{M_i}{\bar{M}} \right) \nabla \ln p = \sum_{k \neq i} \frac{x_i \mathcal{J}_k - x_k \mathcal{J}_i}{D_{ik}} \quad , \tag{21}$$

where D_{ik} is a dimensionless transport property for binary interactions, defined as $D_{ik} = c\, \mathcal{D}_{ik} / c_\infty \nu_\infty$. For a mixture of n species, there are $(n-1)$ independent force balances in the form of Eq. (21), and there are $\frac{1}{2} n(n-1)$ independent transport properties because D_{ii} is not defined and, by Newton's third law of motion, $D_{ik} = D_{ki}$.

A steady-state material balance in the gas phase is

$$\nabla \cdot \underline{N}_i = R_i \tag{22}$$

where R_i is the net homogeneous rate of production of species i.

Equations (21) can be inverted numerically to give explicit expressions for the fluxes, which can then be substituted into Eq. (22) to give a dimensionless material balance,

$$\frac{d^2 x_i}{d\zeta^2} = \sum_{k\neq i}\left[\frac{x_i R_k - x_k R_i}{D_{ik}} - \frac{cH}{c_\infty D_{ik}}\left(x_i \frac{dx_k}{d\zeta} - x_k \frac{dx_i}{d\zeta}\right) + J_k \frac{d}{d\zeta}\left(\frac{x_i}{D_{ik}}\right) - J_i \frac{d}{d\zeta}\left(\frac{x_k}{D_{ik}}\right)\right], \quad (23)$$

for the one dimensionless problem considered here. There are n-1 independent force balances with the form of Eq. (23) which can be used, in conjunction with the relationship between the fluxes

$$\sum_i M_i J_i = 0 \quad , \quad (24)$$

to describe mass transfer in a multicomponent system.

In this way, it is possible to incorporate the conservation conditions while still leaving the overall continuity equation (4) to be counted as one of the hydrodynamic equations. Furthermore, arbitrary selection of one of components is not required in order to replace a species material balance with Eq. (24) or to invert the Stefan-Maxwell relations (21).

At the disk surface, n-1 Stefan-Maxwell relations, Eq. (21), are used, together with the relationship between mole fractions, $\sum_i x_i = 1$. Far from the disk, the compositions approach their equilibrium values at the bulk fluid temperature.

Chemical Reactions

The equations derived above, which describe the transfer of heat, mass, and momentum for a disk rotating in an infinite medium, can be used

to predict the behaviour of systems with an arbitrary number of homogeneous and heterogeneous reactions.

To illustrate the use of this technique, epitaxial deposition of silicon from an input mixture of $SiCl_4$ in excess hydrogen is analysed. Thermodynamic studies indicate that, for the temperature range of interest, five principal species are present in the gas phase; H_2 HCl, $SiCl_4$, $SiHCl_3$, and $SiCl_2$ [12]. Dichlorosilane (SiH_2Cl_2) has also been detected under some experimental conditions, but this species is not considered explicitly in the present study.

Several mechanisms have been proposed for the formation of silicon from $SiCl_4$ [2, 13, 14]. Here, it is assumed that $SiCl_4$ can be reduced either homogeneously or heterogeneously by the following reversible reactions:

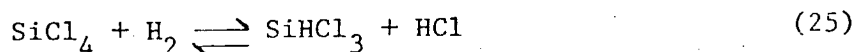

$$SiCl_4 + H_2 \rightleftharpoons SiHCl_3 + HCl \tag{25}$$

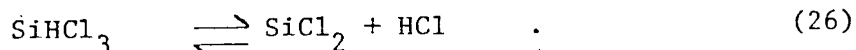

$$SiHCl_3 \rightleftharpoons SiCl_2 + HCl \quad . \tag{26}$$

On the surface, the deposition reaction

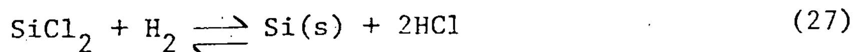

$$SiCl_2 + H_2 \rightleftharpoons Si(s) + 2HCl \tag{27}$$

can also take place. This mechanism may need to be refined subsequently, to match experimentally observed behaviour.

The net rate of each reaction is regarded as the difference between the rates of forward and backward reactions and can be represented as

$$r_\ell = k_{\ell f} \prod_i x_i^{\nu_{i\ell}} - k_{\ell b} \prod_i x_i^{-\nu_{i\ell}} \quad , \tag{28}$$

$$\nu_{i\ell} > 0 \qquad \nu_{i\ell} < 0 \quad .$$

where $k_{\ell f}$ and $k_{\ell b}$ are rate constants for forward and backward reactions, respectively. The exponent $\nu_{i\ell}$ is the stoichiometric coefficient for species i in reaction ℓ. It is positive for reactants and negative for products, and may be obtained from Eqs. (25)-(27), which are assumed to be elementary reaction steps.

The temperature dependence of the rate constants in Eq. (28) is assumed to be given by

$$k_{\ell b} = A_\ell \, e^{-E_\ell/T} \tag{29}$$

where E_ℓ can be regarded as an activation energy for reaction ℓ .

In the model, 5 independent parameters are used to describe the kinetic behaviour: E_a; $\theta_1 = k_{3b}/k_{1b}$; $\theta_2 = k'_{2b}/k'_{1b}$; $\theta_3 = k_{1b}^2 \, e^{E_a/T_s}/c_\infty \nu_\infty \, k'_{1b}$; $\theta_4 = 10^2 \, e^{-E_a/T_s} \, c_\infty \Omega/k'_{2b}$. The term E_a represents an activation energy for the deposition process. Different activation energies could be chosen for each reaction, but it is assumed that the temperature dependence of the deposition rate will be influenced more by the activation energy for the rate-limiting step than by the activation energies for the other reactions. The parameters θ_1 and θ_2 describe the relative rates of the two heterogeneous and the two homogeneous reactions, respectively. θ_3 is a ratio of the rates of the heterogeneous and homogeneous reactions and θ_4 specifies the rate of homogeneous production of $SiCl_2$, as described by Eq. (26), relative to the mass transfer rate characterised by the disk speed, Ω .

The forward and backward rate constants are related by an equilibrium constant $K_\ell = k_{\ell b}/k_{\ell f}$, which is defined in terms of equilibrium reactant

and product compositions as

$$K_\ell = p^m \prod_i x_{ie}^{-\nu_{i\ell}} \tag{30}$$

In Eq. (30), the activity of any solid phase is taken to be unity, and m represents the net number of molecules produced by reaction ℓ. The temperature dependence of k_ℓ is predicted from standard heats of reaction $\Delta H(T)$, with

$$\left[\frac{\partial \ln K_\ell}{\partial (1/T)}\right]_p = -\Delta H(T)/R \; , \tag{31}$$

and from free energy data at 25°C [15], to give expressions of the form:

$$\ln K_\ell = \alpha_\ell + \beta_\ell/T + \gamma_\ell \ln T \quad . \tag{32}$$

The coefficients α_ℓ, β_ℓ, γ_ℓ, used for the reactions are summarised in Table 1.

In the gas phase, the net rate of production of species i is given as

$$R_\ell = \sum_i \nu_{i\ell}\, r_\ell \quad . \tag{33}$$

At the surface, a similar summation for the heterogeneous reactions represents the molar flux $\underline{N}_i$ from the surface relative to the interface. The variables $\underline{N}_i$ and R_i link the rates of the individual reactions to the equations that describe heat, mass, and momentum transfer for the rotating disk.

Interactions among the governing differential equations are caused directly by the inclusion of a finite interfacial velocity (see Eq. (10))

and variable physical properties in the analysis. Relationships for the temperature and composition dependences of physical parameters needed in the model are summarised in the Appendix.

For the example of chemical vapour deposition of silicon, with five species in the gas phase, the steady state behaviour is described by a set of 15 coupled, nonlinear, ordinary differential equations. These equations, subject to specified boundary conditions, can be solved numerically by a finite difference technique accurate to $O(h^2)$ [11, 16, 17]. The model can be used to study the influence of process variables on the rate of silicon deposition and on the profiles for compositions, velocities, and temperature in the diffusion layer. Parameters that must be specified in the model include surface and bulk temperatures, inlet gas composition, disk rotation rate, and operating pressure.

RESULTS AND DISCUSSION

Preliminary computer simulations indicated that pressure variations through the diffusion layer are small and that they do not affect the overall behaviour, significantly. Consequently, results are presented for a constant operating pressure, which is taken to be 1.013 bar. In addition, the influence of bulk gas composition is not considered explicitly in this study, and results are for an inlet gas mixture of 1 mol.% $SiCl_4$ in hydrogen. The values chosen for pressure and composition correspond to standard operating conditions for chemical vapour deposition of silicon [5].

A typical composition profile, with the disk temperature controlled at 1473 K and a bulk gas temperature of 293 K, is shown in Fig. 1. The gas mixture is assumed to be at equilibrium at the bulk temperature, far from the disk. Closer to the surface, the mole fractions alter in response to the specified homogeneous and heterogeneous reactions.

Spectroscopic methods have been used to measure composition profiles in the diffusion layer for silicon deposition in a horizontal channel reactor, where reactant gases flow over the susceptor surface [3, 4]. These measurements indicate the presence of a maximum in $SiCl_2$ concentration approximately 2 mm from the surface. The magnitude of the maximum mole fraction becomes larger further from the leading edge of the crystal. Analogous behaviour is expected with the rotating disk system since smaller rotation rates, and hence larger diffusion layers, should correspond, at least qualitatively, to positions further downstream in the channel flow reactor. This is exemplified by the dashed lines in Fig. 1 which show the position dependence of $SiCl_2$ mole fraction calculated at rotation rates larger and smaller than the base value. In addition, the model predicts a maximum in the $SiHCl_3$ composition profile, at greater distances from the disk surface than the $SiCl_2$ maximum.

Figure 1 is calculated for a particular set of kinetic parameters that give a qualitative match between theoretical and experimental composition profiles. The relative importance of each parameter is discussed below in the context of rotation rate and surface temperature effects. However, it is noted here that in order to obtain a maximum in $SiCl_2$ composition it is necessary to eliminate the possibility for heterogeneous $SiCl_2$

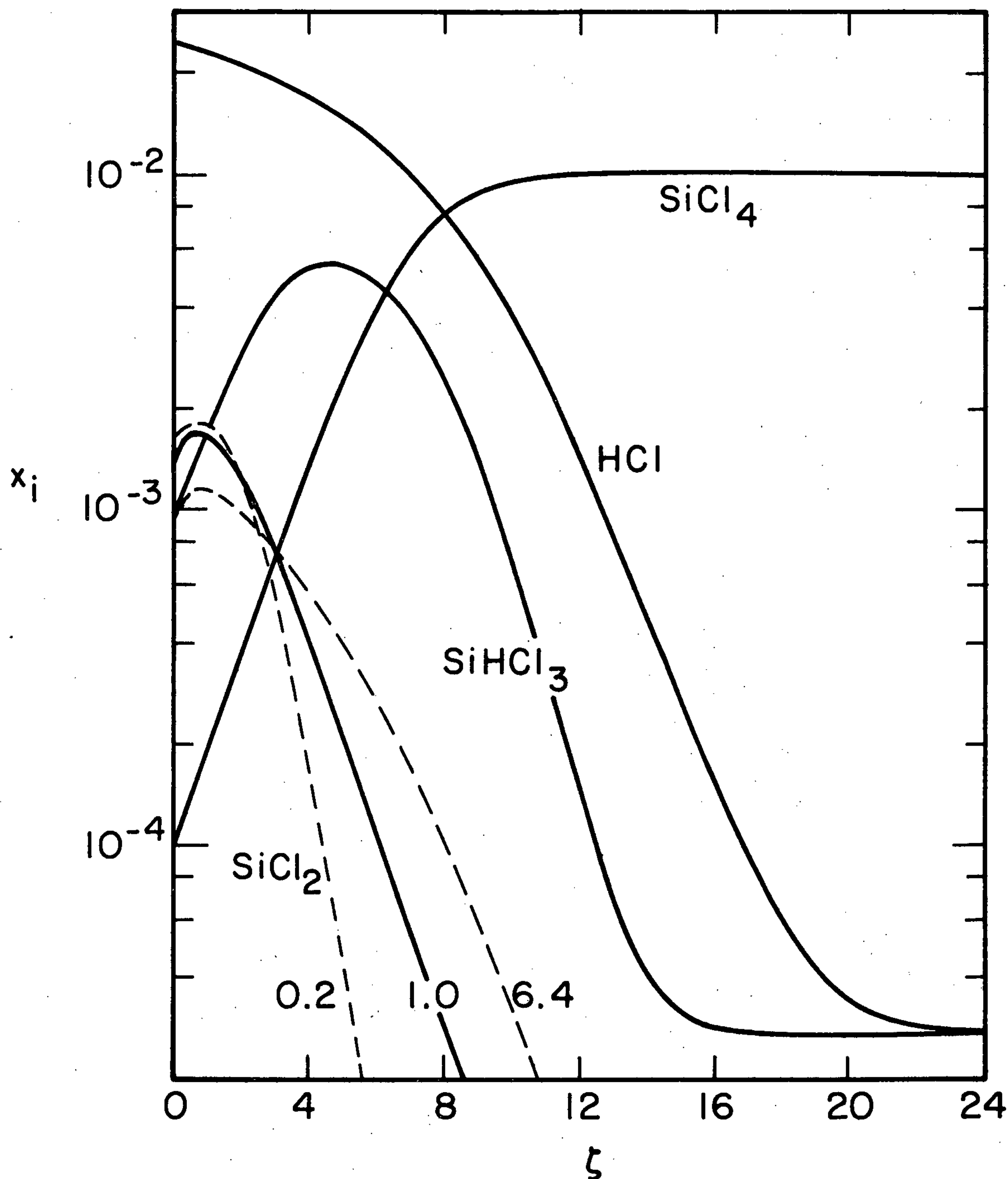

XBL 796-10040

Figure 1. Typical composition profiles in diffusion layer adjacent to rotating disk. Parameter values: T_s = 1473 K; T_∞ = 293 K; Ω_b = 12.57 rad/s; $p_\infty = 1.013 \times 10^5$ N/m^2; $(x_{H_2})_\infty$ = 0.99; θ_1 = 25.0; θ_2 = 10.0; θ_3 = 1.25; θ_4 = 5/6; E_a = 1258.18 K. Dashed lines represent x_{SiCl_2} profiles for different disk speeds, Ω/Ω_b .

production. This is in keeping with some mechanisms that have been postulated for the deposition process.

An approximate estimate of the diffusion layer thichness can be obtained from the composition profiles, even though some species reach their bulk compositions closer to the surface than others. For the example in Fig. 1, an approximate thickness is 5 cm, which is considerably larger than values of 10^{-2} to 10^{-3} cm often encountered with electrolyte solutions.

If the size of the disk and the diffusion layer are comparable, it is necessary to consider the influence of radial effects on observed deposition rates. A singular pertubation analysis of the elliptic region at the edge of a rotating disk that results from radial diffusion has been developed previously for fluids with high Schmidt numbers [18]. This approach can be generalised to give the ratio λ of maximum overall mass transfer rates, with and without radial diffusion effects, as

$$\lambda = 1 + 1.9193\, Re^{-3/4}\, Sc^{-1/2} \tag{34}$$

for any fluid but for large values of $ScRe^{3/2}$. With average values for physical properties and with $\Omega = 12.57$ rad/s and $r_o = 2.5$ cm, it may be shown that $\lambda \simeq 1.1$. This analysis indicates that radial effects can contribute to an increase in overall silicon deposition rate under these conditions, although at higher rotation rates the influence of edge effects will be reduced, in accordance with Eq. (34).

For the operating conditions used in Fig. 1, the variations of some physical properties are shown in Fig. 2. The density changes by a factor

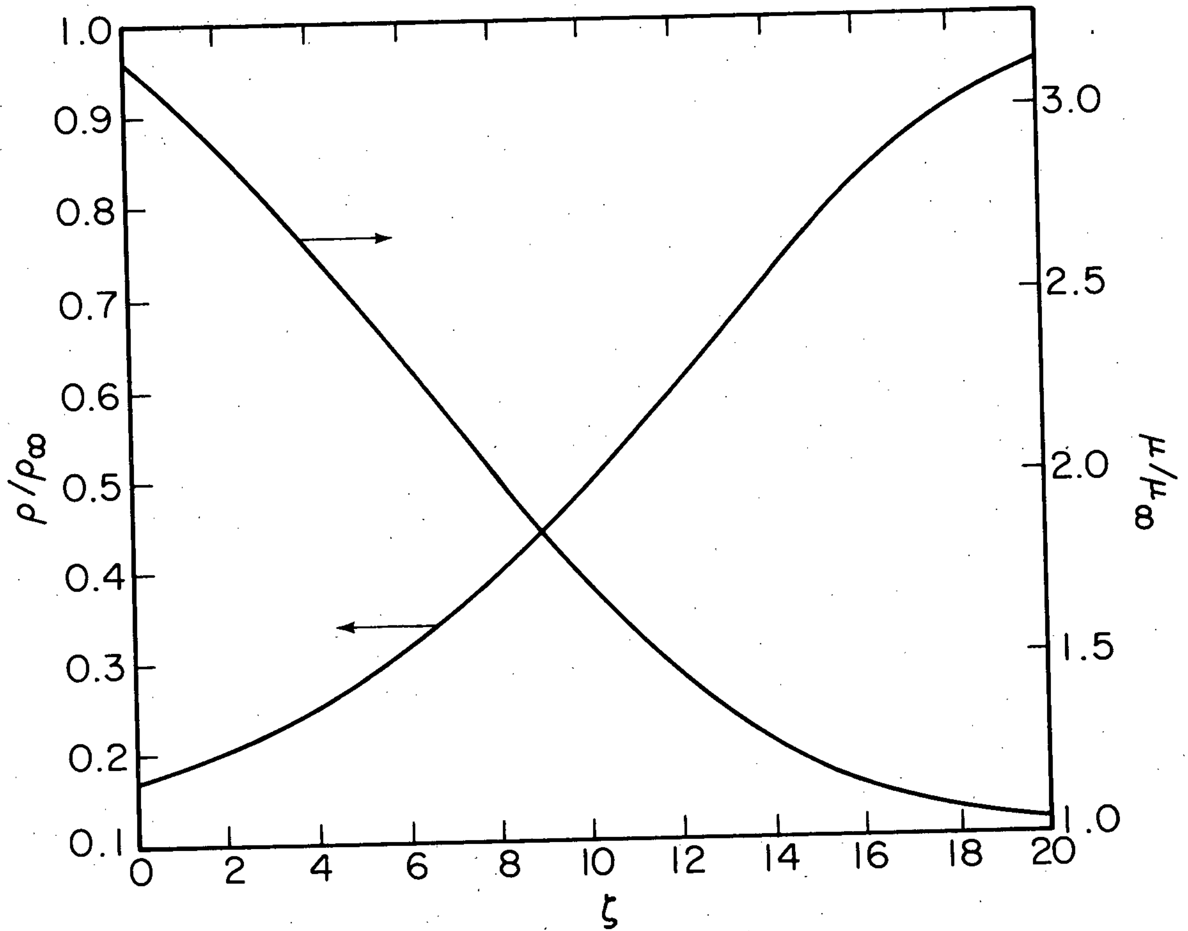

XBL 796-10041

Figure 2. Dependence of viscosity and density on distance from surface of rotating disk. Parameter values as for Figure 1

$\rho_\infty = 0.1536$ kg/m^3; $\mu_\infty = 9.602 \times 10^{-6}$ kg/m.s

of 6 across the diffusion layer in direct association with changes in T and $\bar{M}$. Viscosity and thermal conductivity both vary by factors of about 3. This leads to a maximum in the axial velocity profile in the boundary layer, as illustrated in Fig. 3. In this example, the magnitude of the interfacial velocity, which arises from chemical reactions at the disk surface, is -2.0 mm/s. An assumption of zero interfacial velocity can lead to errors of approximately 1 to 6% in deposition rate, dependent on the process conditions.

Measurements of silicon deposition rates at various susceptor temperatures and for a fixed rotation speed show that there are two regimes of temperature bahaviour in the range 1273 K - 1523 K. At higher temperatures an apparent activation energy for deposition lies in the range 4-13 kJ/mol, whereas at lower temperatures it is reported as 90 - 125 kJ/mol [7]. This change in temperature dependence is attributed to a shift from reaction rate control to mass transfer control as the disk temperature is raised.

An experimental curve, obtained with a rotation rate of 12.5 rad/s , is given in Fig. 4, where the parameter S represents the actual deposition rate, made dimensionless with the quantity $c_\infty \sqrt{\nu_\infty \Omega}$. The dashed line is the locus of maximum deposition rates calculated with the mathematical model. It can be regarded as a combined thermodynamic-mass transfer limit since, for this curve, the reactions are locally at equilibrium but the finite mass transfer rate through the diffusion layer limits the fraction of the bulk fluid that can reach the disk surface.

There are several possible explanations for the discrepancy between the thermodynamic-mass transfer limit and experimental results at high

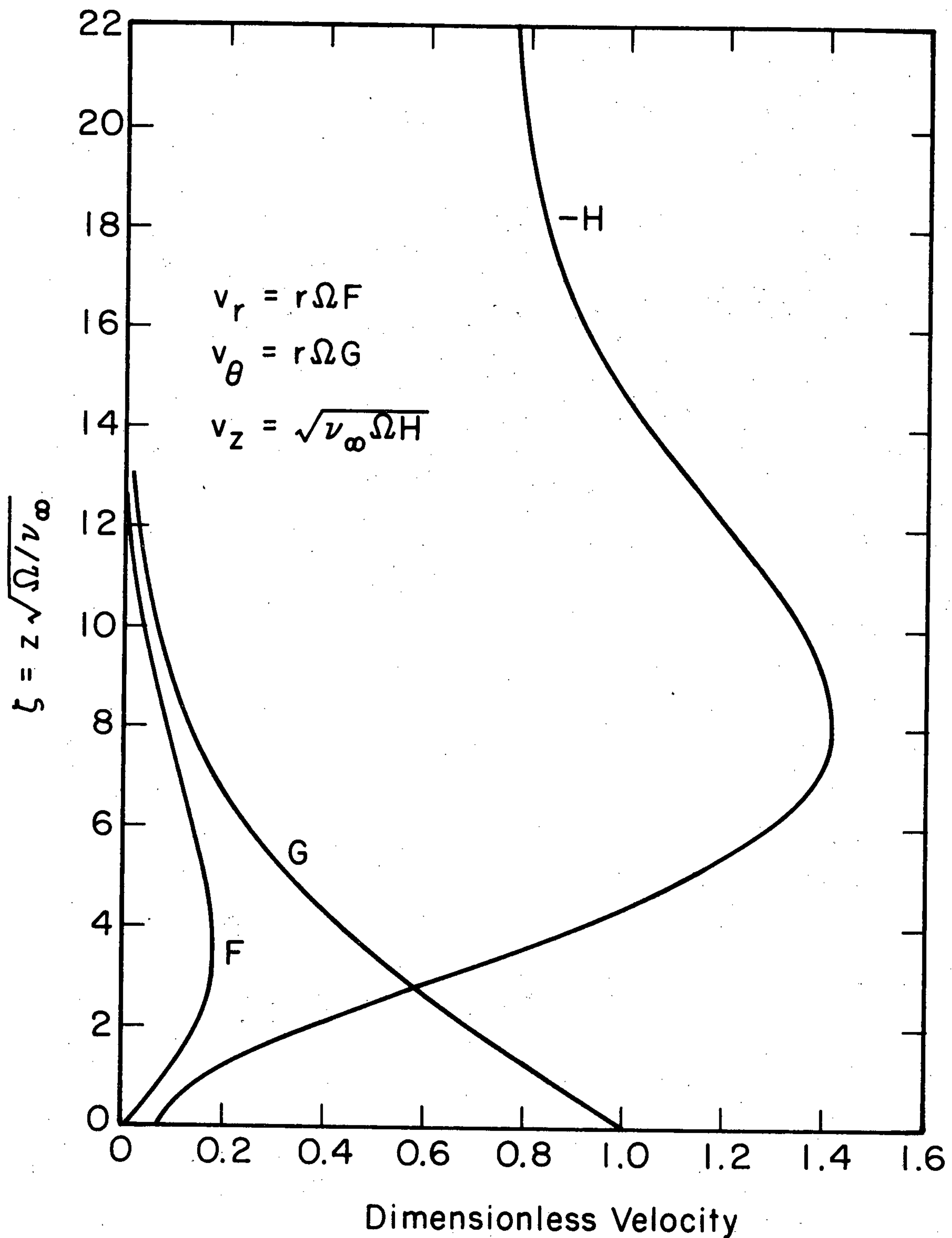

XBL 796-10042

Figure 3. Velocity profiles for silicon deposition on a rotating disk. Parameter values as for Figures 1 and 2.

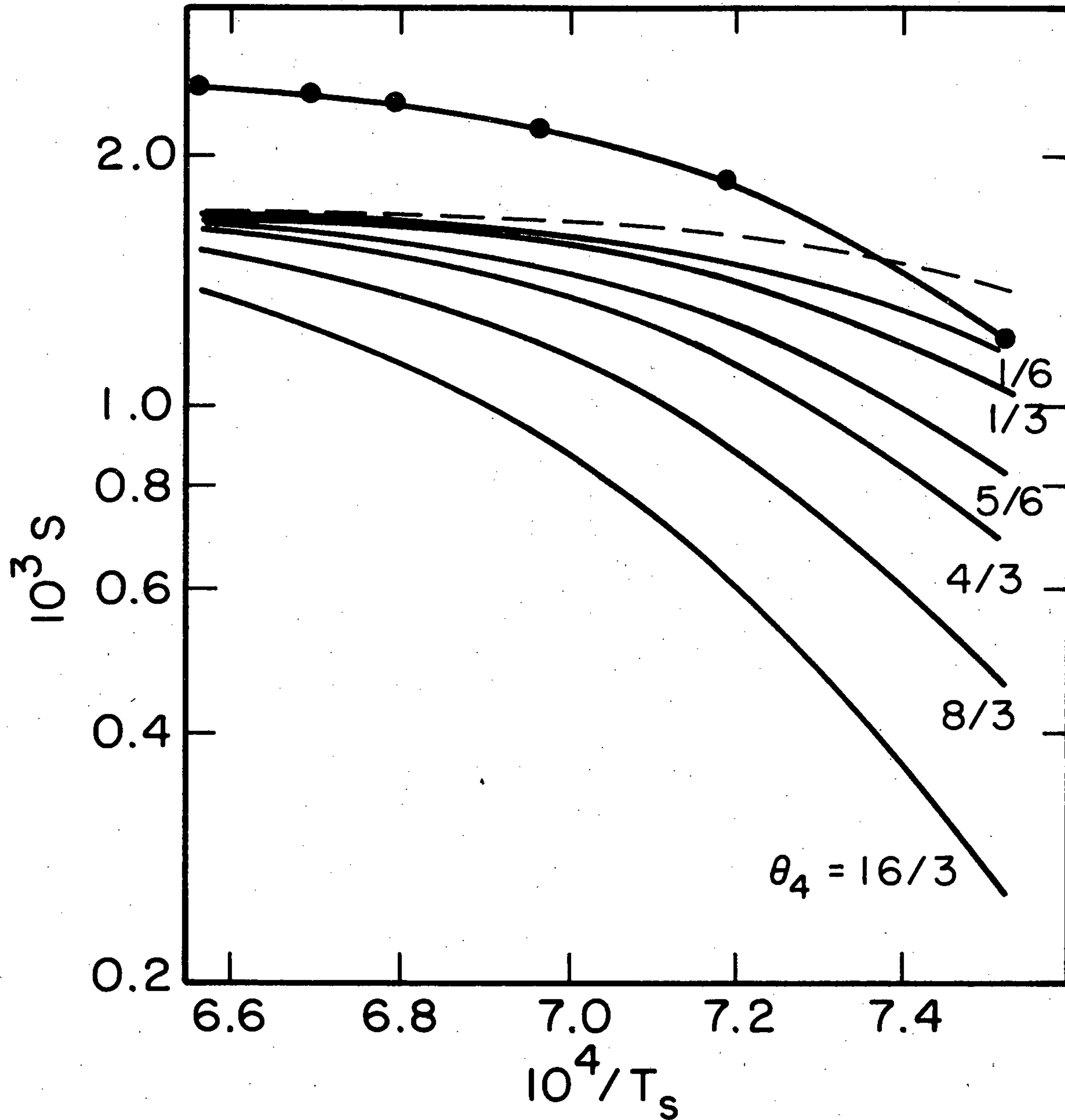

XBL 796-10043

Figure 4. Dependence of dimensionless silicon deposition rate on disk temperature. S = actual deposition rate/$c_\infty\sqrt{\nu_\infty\Omega}$. Dotted line: experimental data (7), Ω = 12.57 rad/s . Dashed curve: thermodynamic-mass transfer limit for deposition rate. Full curves: theoretical predictions for different values of θ_4, with other parameters as in Figures 1-3.

temperatures. Firstly, errors in estimates of collision diameters and interaction energies for some combinations of species could lead to incorrect predictions of physical properties such as diffusion coefficients and viscosity (see Appendix). Errors may also arise from incorrect predictions of equilibrium constants (see Table 1). A thermodynamic evaluation of the Si-H-Cl system shows that the parameters K_ℓ are particularly sensitive to the standard heat of formation of $SiHCl_3$ [12].

Radial effects can lead to enhanced mass transfer rates. However, it has been shown (see below Eq. (34)) that the magnitude of this effect is insufficient to account fully for the differences between experiment and theory. Nevertheless, it should be noted that the analysis of radial dependences does not consider the influence of hydrodynamic disturbances that could arise from axial motion at the disk edge.

Even though inlet gases are at 293 K, the wall temperature in the experiment is recorded as 673 K [7] and heat transfer between the disk and walls and the inlet gas (eg. by radiation) could raise the bulk gas temperature substantially. Figure 5 shows the temperature dependence of dimensionless deposition rate with T_∞ = 673 K. The discrepancy between experimental results and the thermodyanmic-mass transfer limit is reduced with this new boundary condition, but significant differences still exist.

Another possible explanation for the enhanced mass transfer rate is natural convection. The ratio

$$\frac{Gr}{Re^2} = \frac{(T_s - T_\infty)g}{T_{av}\Omega^2 r_o} \qquad (35)$$

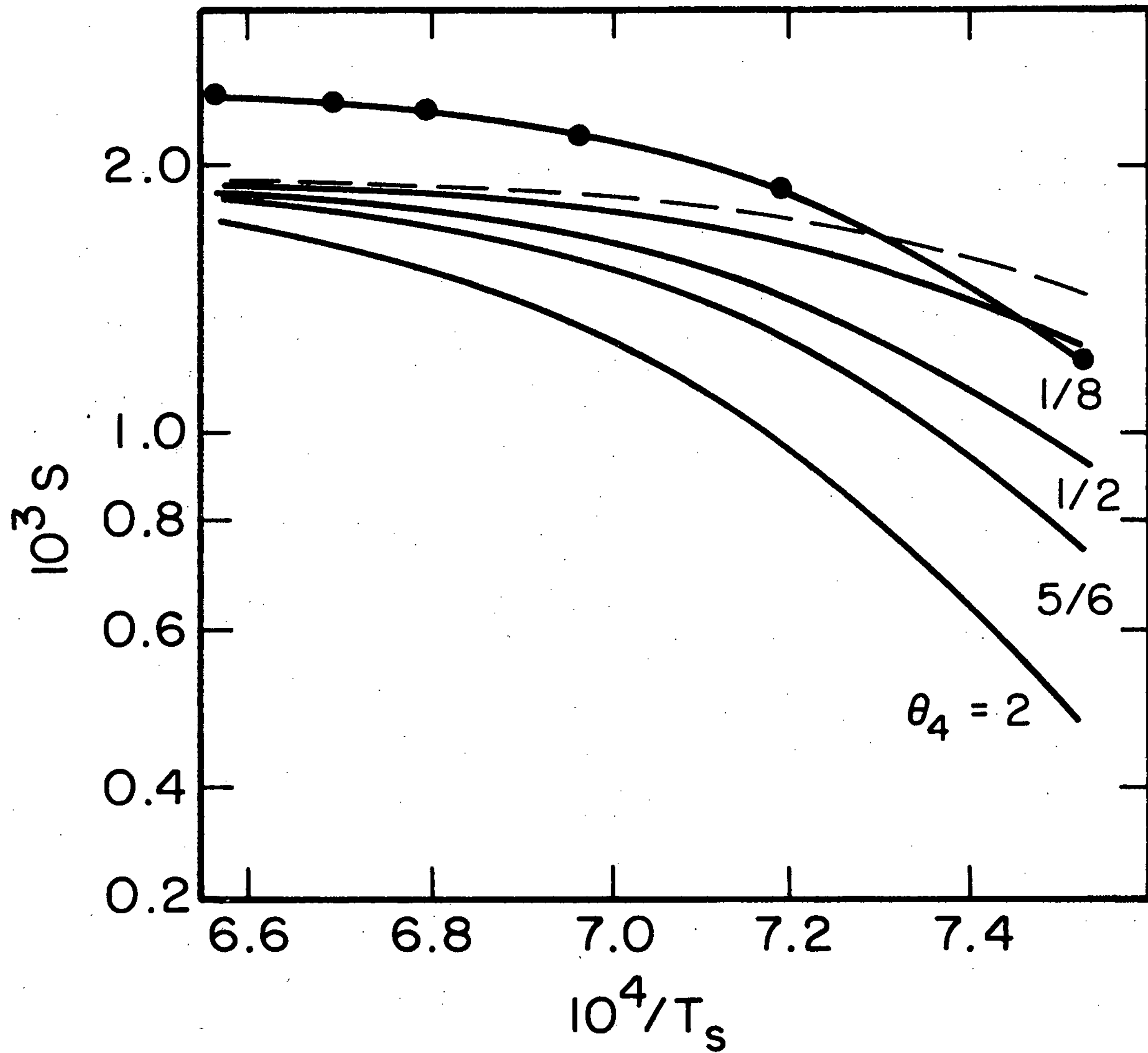

XBL 796-10044

Figure 5. Dependence of dimensionless silicon deposition rate on disk temperature. As Figure 4, but $T_\infty = 673$ K .

can be used to represent the ratio of bouyancy forces to viscous forces in the system. With $T_s - T_\infty = 1200$ K, $T_{av} = 1000$ K, $r_o = 2.5$ cm, and $\Omega = 12.57$ rad/s, this ratio is approximately 3.0. For an upward-facing disk, it has been shown [1] that natural convection is the dominant heat transfer mechanism for $Gr/Re^2 > 4.1$ and that forced convection dominates when $Gr/Re^2 < 0.4$. Consequently, for the disk considered in the example, there will be a transition region for $10.72 < \Omega$ (rad/s) < 34.31. Unfortunately, experimental information for silicon deposition on a rotating disk is only available for conditions where natural convection could be important. Therefore an exact match between experimental results and theoretical predictions based on forced convection should not be expected. Nevertheless, under different conditions, such as larger disks and higher rotation rates, the model presented will have greater quantitative significance.

Despite the uncertainty in the absolute magnitude of the deposition rate, Figs. 4 and 5 both show that the thermodynamic-mass transfer limit does not adequately explain the temperature dependence of the deposition rate over the whole temperature range considered. With finite kinetic parameters it is possible to obtain a satisfactory match between the shapes of the the theoretical and experimental curves. In Figs. 4 and 5, the kinetic parameters θ_1, θ_2, θ_3 and E_a are fixed, and θ_4 is varied. The sets of curves can be interpreted as showing the effect of variations either in rotation rate at fixed k_2' or in k_2' at fixed Ω. Inspection of Fig. 4 ($T_\infty = 293$ K) shows that a value of $\theta_4 = 5/6$ provides a reasonable fit between the shapes of the experimental and theoretical curves.

As the surface temperature is decreased, the $\theta_4 = 5/6$ curve moves away from the thermodynamic-mass transfer limit and the deposition rate becomes more dependent on kinetic factors. However, as T_s is reduced further, equilibrium limitations are expected to become important again and eventually, below a surface temperature of approximately 1108 K, silicon deposition will no longer be thermodynamically feasible.

It is necessary to consider the sensitivity of the results to the values chosen for the kinetic parameters. Figures 6 and 7 show predicted temperature dependences for different values of E_a, with fixed values of θ_1 and θ_2 and with the value of θ_3 matched at 1473 K for the different activation energies. The diagrams show that the overall shapes of the curves do not depend noticeably on E_a for $0 \leq E_a \leq 6290.90$.

Variations in θ_1 and θ_3 cause relatively small changes in calculated temperature profiles, for fixed values of θ_2, θ_4, and E_a. Changes in θ_2 have a more noticeable effect but, as with alterations in E_a, it merely shifts the value of θ_4 which best fits the shape of the experimental curve. From these results it is evident that the dependence of silicon deposition rate on temperature alone is insufficient to be able to predict most appropriate values for the kinetic parameters.

Information is also available on the dependence of deposition rate on disk speed [7]. Figure 8 shows experimental results and theoretical predictions with the same kinetic parameters (θ_1,θ_2,θ_3, E_a) that were used in Fig. 4. The deposition rate S_b is made dimensionless with a specified rotation rate Ω_b which is taken as 26.18 rad/s, close to the midpoint in the range of experimental data. The parameter Ω_s, which equivalent to θ_4,

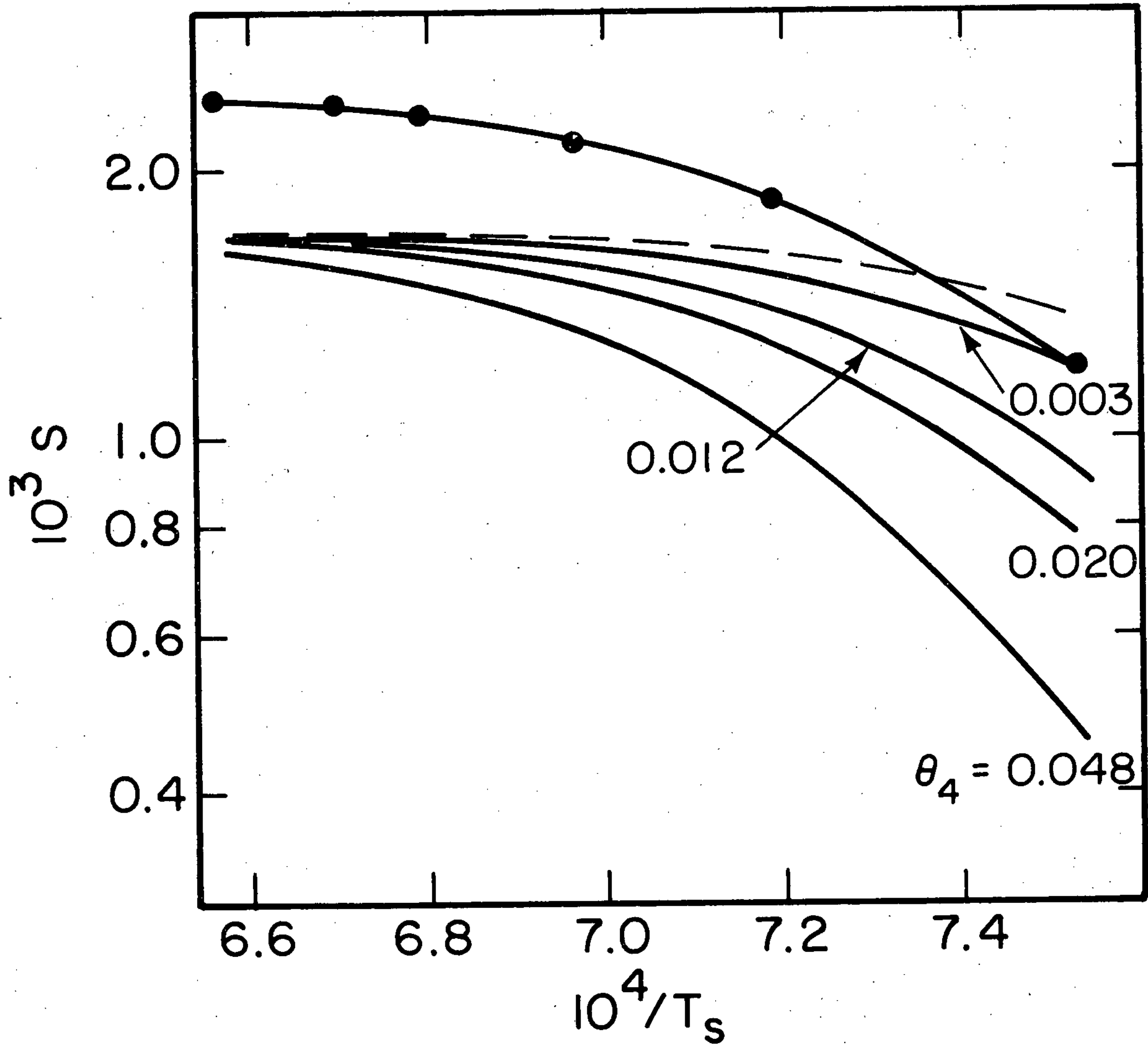

Figure 6. Dependence of dimensionless silicon deposition rate on disk temperature. As Figure 4, but E_a = 6290.90 K and θ_3 = 38.071 .

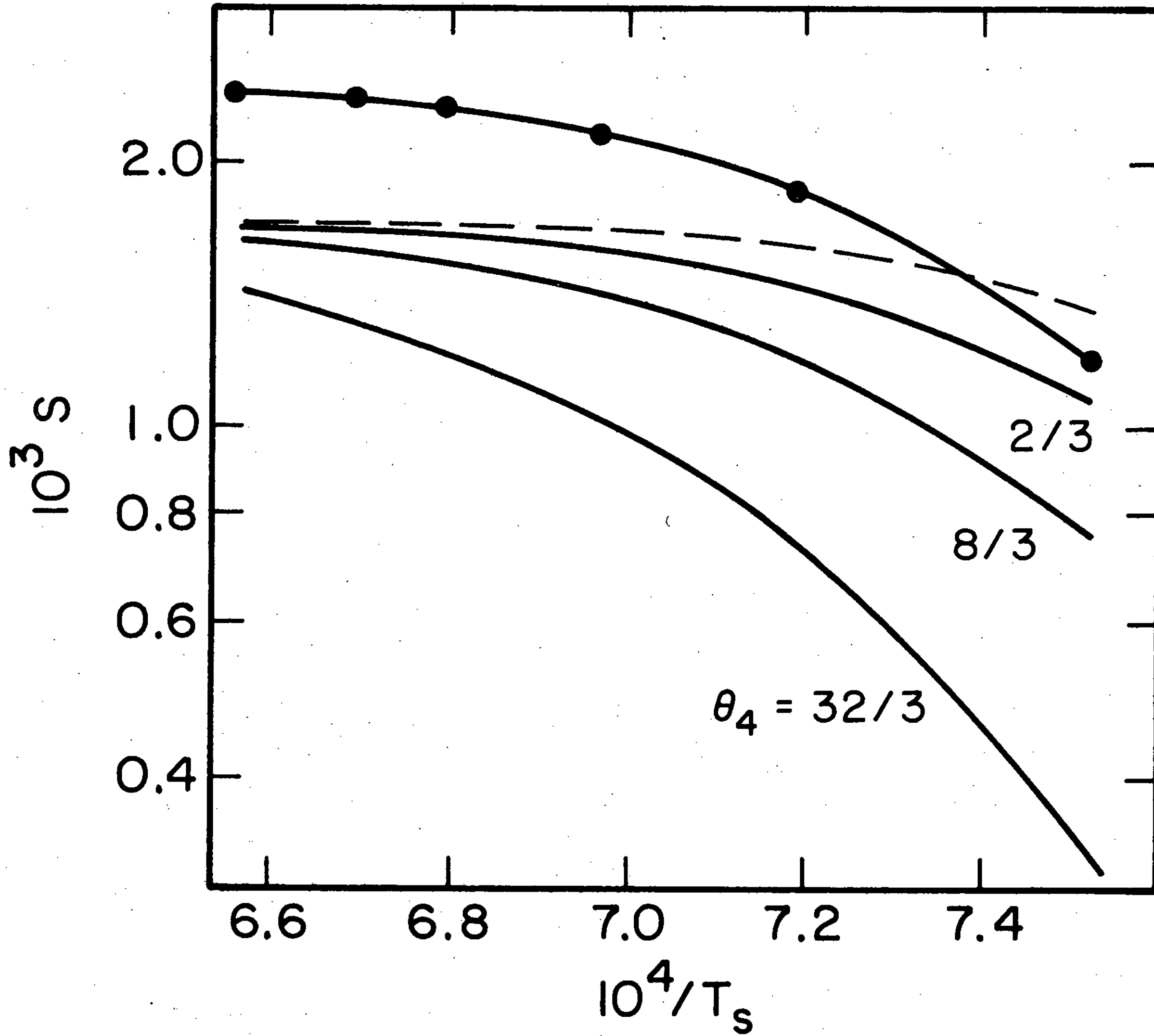

XBL 796-10046

Figure 7. Dependence of dimensionless silicon deposition rate on disk temperature. As Figure 4, but $E_a = 0$ and $\theta_3 = 0.5321$.

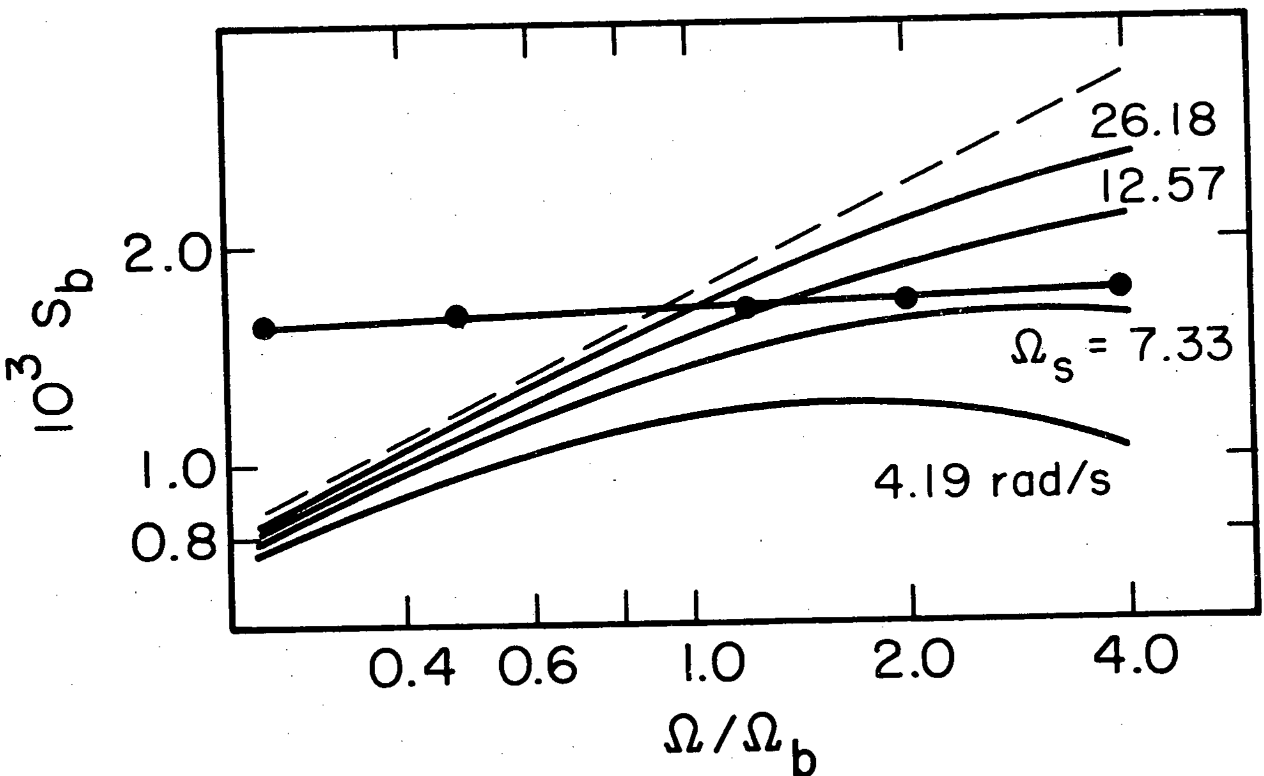

XBL 796-10047

Figure 8. Dependence of dimensionless silicon deposition rate on disk speed. $S_b = \sqrt{\Omega/\Omega_b}$. Dotted line: experimental data $T_s = 1473$ K . Dashed curve: thermodynamic-mass transfer limit for deposition rate. Full curves: theoretical predictions for different values of Ω_s (equivalent to θ_4) . Parameter values: $T_s = 1473$ K; $T_\infty = 293$ K; $\Omega_b = 26.18$ rad/s; $p_\infty = 1.013 \times 10^5$ N/m^2; $(x_{H_2})_\infty = 0.99$; $\theta_1 = 25.0$; $\theta_2 = 10.0$; $\theta_3 = 1.25$; $E_a = 1258.18$ K .

represents the rotation rate which corresponds to the curve that best fits the shape of the data in Fig. 4. (For example, a stipulation that the best curve in Fig. 4 has a rotation rate of 12.57 rad/s yields the curve Ω_s = 12.57 rad/s on Fig. 8). From the standpoint of temperature dependence, it would seem most acceptable to choose Ω_s = 12.57, since this is the rotation rate at which the experiments were performed. However, this curve follows the thermodynamic-mass transfer limit too closely in Fig. 8 and does not match the experimental data, which are almost independent of rotation rate.

At low speeds, mass transfer control might be expected, as illustrated by the thermodynamic-mass transfer limit ($S_b \alpha \sqrt{\Omega}$), whereas at higher speeds the rotation rate dependence could change markedly as reaction rate control is approached. A higher disk speed not only raises the rate at which reactants can reach the disk surface, but it also affects the rate at which intermediate species in the reaction sequence can be convected away from the disk. In addition, the relative importance of the homogeneous and heterogeneous reactions can shift as Ω is changed. Consequently, it is conceivable that, under some circumstances, an increase in Ω could lead to a reduction in deposition rate.

These effects become apparent as the parameter is reduced below Ω_s = 12.57 rad/s. At Ω_s = 7.33 rad/s, the theoretical curve rises from the thermodynamic-mass transfer limit to the experimental line as the rotation rate is increased. Below 26.18 rad/s, the experimentally observed behaviour cannot be matched because the results lie above the predicted limit. This may be due to error in the assessment of the thermodynamic-

mass transfer curve as discussed earlier and, in particular, it might result from natural convection which would be expected to be more important at low disk speeds. Therefore, it is possible that, for these experimental conditions, there is no range of rotation rates for which forced convection mass transfer controls the system behaviour. Furthermore, Fig. 8 is practically unchanged for modest changes in kinetic parameters, and it is not possible to choose different values for θ_1 to θ_4 or E_a which would provide a substantially better fit of the experimental data. It should also be noted that natural convection could alter the shapes of the temperature curves in Fig. 4, as well as the absolute value of the thermodynamic-mass transfer limit.

Notwithstanding the possible influence of natural convection, prediction of a consistent set of kinetic parameters, which fit the observations, is hampered by the relatively short ranges of T_s and Ω for which data are available. Also the surface temperature in Fig. 8 lies, ostensibly, in a mass-transfer controlled region, and therefore one should not expect to be able to use this information to obtain well-defined kinetic information. In principle, it should be possible to use experimental data in the reaction controlled regime to obtain better estimates of the kinetic constants.

It is also necessary to assess the extent to which the predicted behaviour is influenced by the assumed reaction mechanism. The mechanism proposed includes homogeneous and heterogeneous production of $SiHCl_3$, homogeneous decomposition of $SiHCl_3$ to give $SiCl_2$, and reduction of $SiCl_2$ on the disk surface to yield silicon. Under some circumstances, significant quantities of SiH_2Cl_2 can be present in the gas phase [12]. This could

be produced by

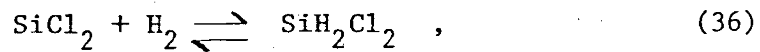

$$SiCl_2 + H_2 \rightleftharpoons SiH_2Cl_2 \quad , \tag{36}$$

and it could decompose on the surface to give silicon directly. Consequently, it might be regarded as an intermediate in the overall conversion of $SiCl_2$ to silicon so that inclusion of SiH_2Cl_2 in the model would not be expected to alter the predictions significantly. Incorporation of SiH_2Cl_2 as an additional species would not cause operational difficulties with the model but it would necessitate additional equilibrium data and consideration of another independent kinetic parameter.

Direct reactions of the form

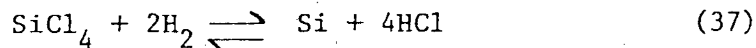

$$SiCl_4 + 2H_2 \rightleftharpoons Si + 4HCl \tag{37}$$

have not been included because they are kinetically less favorable than the elementary processes used in the analysis. An addition reaction which could be included in more sophisticated studies of reaction mechanisms involves disproportionation of $SiCl_2$ according to

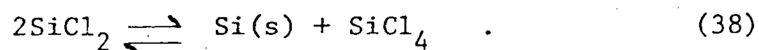

$$2SiCl_2 \rightleftharpoons Si(s) + SiCl_4 \quad . \tag{38}$$

Again, an additional kinetic parameter would be needed in the model.

The rate determining step for the reaction sequence considered (Equations (25)-(27)) is thought to be homogeneous production of $SiHCl_3$ (Eq. (25)). Heterogeneous formation of $SiHCl_3$ becomes more important when the bulk gas temperature is higher. The basis for this postulate is that, for the range of T_s and Ω considered, the relative rate of the

backward and forward reaction was consistently smallest for this step. This theory is supported by observations of higher deposition rates from $SiHCl_3$, rather than $SiCl_4$, under parallel experimental conditions [19].

CONCLUSIONS

A model has been developed which describes the interactions among hydrodynamics, multicomponent heat and mass transport, and reaction kinetics for the rotating disk system. The analysis includes variable physical properties, finite interfacial velocity, and simultaneous homogeneous and heterogeneous reactions.

This model has been used to study chemical vapour deposition of silicon from $SiCl_4$ in excess hydrogen. The influence of disk speed and temperature on the silicon deposition rate have been investigated, and several features of the process have been elucidated:

(i) The diffusion layer thickness is 1 to 10 cm, which is considerably larger than values commonly encountered for liquid systems. Nevertheless, radial diffusion does not affect predicted mass transfer rates markedly.

(ii) Physical properties, such as density and viscosity, vary by factors of between 3 and 6, through the diffusion layer. This distorts the fluid flow profile and gives a maximum in the axial velocity.

(iii) With five gas-phase species and a set of five independent kinetic parameters, the shape of the predicted temperature dependence of deposition rate matches experimental results. At high surface temperatures, a combined mass transfer and thermodynamic limit controls the deposition

rate, but as the disk temperature is lowered kinetic limitations gradually became more important. At much lower temperatures, thermodynamic considerations again dominate, and deposition is no longer feasible below approximately 1108 K. However, effects not included in the model, such as natural convection, could be responsible for discrepancies in absolute magnitudes of predicted and observed deposition rates and in the influence of disk speed on the system behaviour. Furthermore, the kinetic parameters cannot be specified uniquely from the limited experimental data available.

(iv) Homogeneous and heterogeneous reactions are both important in chemical vapour deposition of silicon. For the range of conditions studied, the rate limiting step is found to be formation of the intermediate species $SiHCl_3$, by reduction of $SiCl_4$.

ACKNOWLEDGEMENT

This work was supported by the Division of Solar, Geothermal, Electric and Storage Systems, Office of the Assistant Secretary for Energy Technology, U.S. Department of Energy under contract No. W-7405-Eng-48.

REFERENCES

1. R. Takahashi, Y. Koga, and K. Sugawara, Gas flow pattern and mass transfer analysis in a horizontal flow reactor for chemical vapor deposition, J. Electrochem. Soc. 119, 1406-1412 (1972).
2. V. S. Ban and S. L. Gilbert, Chemical processes in vapor deposition of silicon, Ibid. 122, 1382-1388 (1975).
3. V. S. Ban, Mass spectrometric studies of chemical reactions and transport phenomena in silicon epitaxy, Proc. 6th. Int. Conf. Chemical Vapor Deposition, pp. 66-77 (1977) (The Electrochemical Society, Proceedings volume 77-5).
4. T. O. Sedgwick, G. V. Arbach, and R. Ghez, Formation of $SiCl_2$ in Si epitaxial growth systems, Ibid., pp. 78-89 (1977).
5. C. W. Manke and L. F. Donaghey, Analysis of transport processes in vertical cylinder epitaxy reactors, J. Electrochem. Soc., 124, 561-569 (1977).
6. D. R. Olander, Variable property, interfacial velocity and multicomponent diffusion-effects in the transport-limited reaction of iodine and germanium, Ind. Eng. Chem. Fundamentals, 6, 188-193 (1967).
7. K. Sugawara, Silicon epitaxial growth by rotating disk method, J. Electrochem. Soc., 119, 1749-1760 (1972).
8. Th.v. Kármán, Über laminare und turbulente Reibung, Z. Angew. Math. Mech., 1, 233 -252 (1921).
9. J. Newman and L. Hsueh, The effect of variable transport properties on mass transfer to a rotating disk, Electrochim. Acta, 12, 417-427 (1967).

10. R. B. Bird, W. E. Stewart, and E. N. Lightfoot, Transport Phenomena, John Wiley, New York (1960).

11. J. S. Newman, Electrochemical Systems, Prentice-Hall, Inc., Englewood Cliffs, N.J. (1973).

12. L. P. Hunt and E. Sirtl, A thorough thermodynamic evaluation of the silicon-hydrogen-chlorine system, J. Electrochem. Soc., 119, 1741-1745 (1972).

13. E. Sirtl, L. P. Hunt, and D. H. Sawyer, High temperature reactions in the silicon-hydrogen-chlorine system, J. Electrochem. Soc., 121, 919-925 (1975).

14. J. Nishizawa and N. Nihira, Mechanisms of chemical vapor deposition of silicon, J. Crystal Growth, 45, 82-89 (1978).

15. D. R. Stull and H. Prophet, Editors, JANAF Thermochemical Tables, National Bureau of Standards, Washington D. C. NSRDS-NBS 37 (1971).

16. J. Newman, Numerical Solution of Coupled, Ordinary Differential Equations, Industrial and Engineering Chemistry Fundamentals, 7, 514-517 (1968).

17. R. E. White, On Newman's Numerical Technique for Solving Boundary Value Problems, Ibid., 17, 367-369 (1978).

18. W. H. Smryl and J. Newman, Limiting current on a rotating disk with radial diffusion, J. Electrochem. Soc. 118, 1079-1081 (1971).

19. V. S. Ban, Chemical Processes in vapor deposition of silicon, J. Electrochem. Soc., 122, 1389-1391 (1975).

20. C. R. Wilke, The Viscosity Equation of Gas Mixtures, J. Chem. Phys., 18, 517-519 (1950).

APPENDIX

Physical Properties

Viscosity

The temperature dependence of the viscosity of each species in the gas phase is predicted from the Chapman-Enskog kinetic theory [10].

$$\mu_i = \frac{2.6693 \times 10^{-5}\sqrt{M_i T}}{\sigma_i^2 \, \Omega_{\mu_i}} \tag{39}$$

The parameter σ_i is the collision diameter, and Ω_{μ_i} is a dimensionless function which depends on kT/ε_i where ε_i is a characteristic energy of interaction between molecules and k is Boltzmann's constant. For each species, Eq. (39) is rewritten in the simplified form

$$\mu_i = \delta_{1i} T^{\psi_{1i}} \quad , \tag{40}$$

and values for δ_{1i} and ψ_{1i} are given in Table 2. The viscosity of the gas mixture is calculated with the Wilke correlation [20],

$$\mu_{mix} = \sum_{i=1}^{n} (x_i \mu_i / \sum_{j=1}^{n} x_i \Phi_{ij}) \quad , \tag{41}$$

where $\Phi_{ij} = [\, 1 + (\mu_i/\mu_j)^{1/2} \, (M_j/M_i)^{1/4}]^2 / [8 + 8 \, M_i/M_j]^{1/2}$.

Diffusivity

Diffusion coefficients for binary interactions are estimated from [10],

$$\frac{c\mathcal{D}_{ij}}{\sqrt{T}} = \frac{2.2646 \times 10^{-5} \left(\frac{1}{M_i} + \frac{1}{M_j}\right)^{1/2}}{\sigma_{ij}^2 \, \Omega_{\mathcal{D}_{ij}}} \tag{42}$$

where σ_{ij} is a mean collision diameter which is taken as $(\sigma_i + \sigma_j)/2$. The dimensionless quantity $\Omega_{\mathcal{D}_{ij}}$ is analogous to Ω_{μ_i} used for the viscosity calculations, but the characteristic of the intermolecular potential field should now represent both species i and j , and is assumed to be given by $\varepsilon_{ij} = \sqrt{\varepsilon_i \varepsilon_j}$. Figure 9 shows the temperature dependence of diffusion coefficients obtained from Eq. (42). In the analysis, a simplified form

$$c\,\mathcal{D}_{ij} = B_{ij} T^{\ell_{ij}} \qquad (43)$$

is chosen with parameters which best fit the curves in Eq. 9 over the temperature range of interest (see Table 3).

Specific Heat

The temperature dependence of the heat capacity of each species is obtained from

$$\tilde{\tilde{C}}_{pi} = \alpha_i + \beta_i T + \gamma_i T^2 \quad , \qquad (44)$$

where the coefficients are summarised in Table 4.

Thermal Conductivity

Eucken's equation for polyatomic gases [10]

$$k_i = (\tilde{C}_{pi} + 5R/4)\,\frac{\mu_i}{M_i} \qquad (45)$$

is used to relate the thermal conductivity and viscosity of each species at a given temperature. An approximately relationship

$$k_i = \delta_{2i} T^{\psi_{2i}} \qquad (46)$$

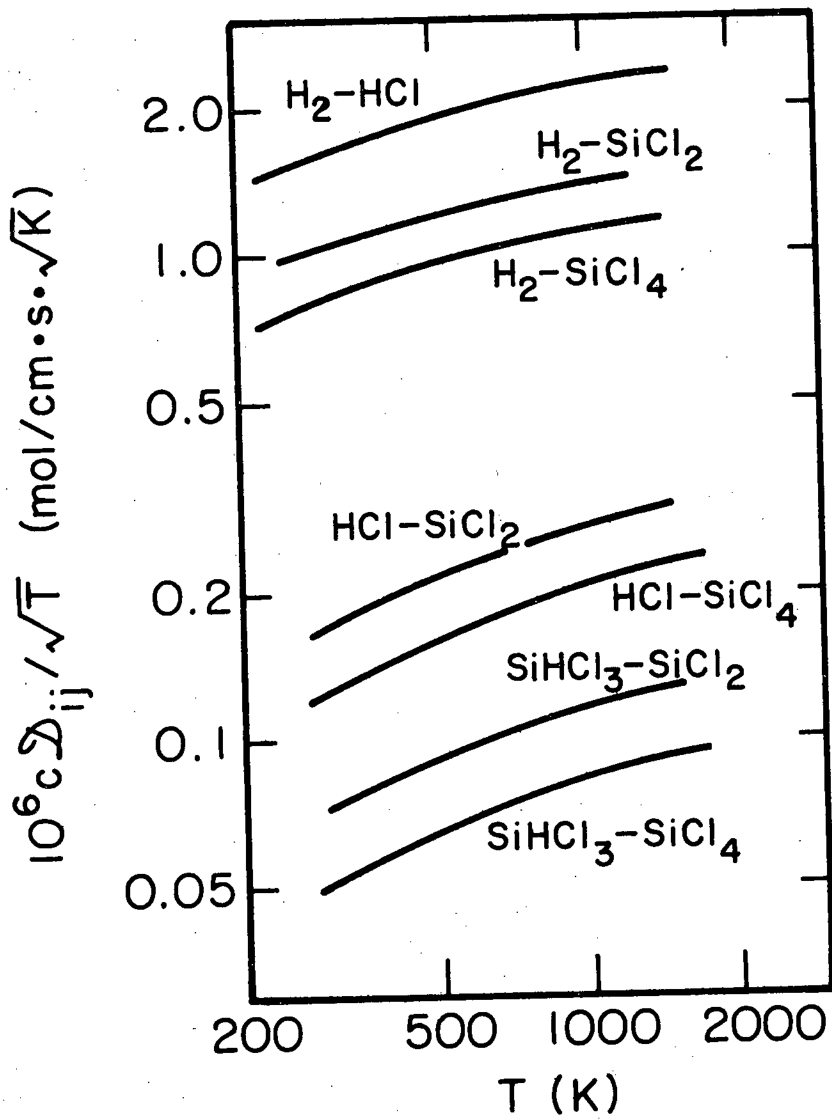

XBL 796-10048

Figure 9. Temperature dependence of binary diffusion coefficients.

is then used to describe the temperature dependence of k_i (see Table 2). The thermal conductivity of the mixture is given by an expression analogous to Eq. (41):

$$k_{mix} = \sum_{i=1}^{n} (x_i k_i / \sum_{j=1}^{n} x_j \Phi_{ij}) \qquad (47)$$

where $\Phi_{ij} = [1 + (k_i/k_j)^{1/2} (M_j/M_i)^{1/4}]^2/[8 + 8 M_i/M_j]^{1/2}$

Nomenclature

A_ℓ	preexponential factor for backward rate constant
c	total concentration (mol/cm^3)
c_i	concentration of species i (mol/cm^3)
C	Dimensionless total concentration, c/c_∞
$\tilde{C}_p$	Molar heat capacity of mixture (J/mol. K)
$\tilde{C}_{pi}$	molar heat capacity of species i (J/mol. K)
$\mathcal{D}_{ik}$	diffusion coefficient for binary interactions (cm^2/s)
D_{ik}	dimensionless diffusion coefficient for binary interactions
D_k^T	thermal diffusivity for species k (kg/m.s)
E_a	kinetic parameter representing activation energy of rate-limiting step (K)
E_ℓ	activation energy for reaction ℓ (K)
F	dimensionless radial velocity defined in Eq. (1)
g_z	gravitational acceleration in z direction (m/s^2)
G	dimensionless angular velocity defined in Eq. (1)
Gr	Grashof number
h	mesh size (m)
H	dimensionless axial velocity defined by Eq. (1)
$\bar{H}_i$	partial molar enthalpy of species i (J/mol)
$\tilde{H}_i^*$	molar enthalpy of ideal gas (J/mol)

$\underline{\underline{I}}$ unit matrix

$\underline{J}_i$ flux of species i relative to mass average velocity ($mol/m^2.s$)

J_i dimensionles $\underline{J}_i$

k Boltzmann constant (1.3806×10^{-23} J/K)

k_i thermal conductivity of species i (W/m.K)

$k_{\ell f}$ forward rate constant for reaction ℓ

$k_{\ell b}$ backward rate constant for reaction ℓ

$k'_{\ell b}$ backward rate constant for homogeneous reaction ℓ

K_{ℓ} equilibrium constant for reaction ℓ

m exponent in Eq. (5)

M_i molecular weight of species i

$\bar{M}$ average molecular weight

$\underline{N}_i$ flux of species i ($mol/m^2.s$)

p gas pressure (N/m^2)

P dimensionless gas pressure

Pr Prandtl number

r radial coordinate (m)

r_{ℓ} rate of reaction ℓ

r_o disk radius (m)

R universal gas constant (8.3143 J/mol. K)

Re Reynolds number

R_i rate of homogeneous production of species i ($mol/m^3.s$)

$\mathcal{R}_i$ dimensionless R_i

s dimensionless parameter defined by Eq. (18)

S dimensionless silicon deposition rate

Sc Schmidt number

$\bar{S}_i$ partial molar entropy (J/mol.K)

T temperature (K)

U dimensionless parameter defined by Eq. (19)

$\underline{v}$ mass average velocity (m/s)

v_r radial velocity (m/s)

v_θ angular velocity (m/s)

v_z axial velocity (m/s)

x_i mole fraction of species i

z axial distance from disk surface (m)

Greek symbols

ε_{ij} maximum energy of attraction between molecules i and j (J)

ζ dimensionless axial distance coördinate defined by Eq. (2)

θ_k dimensionless kinetic parameter (k = 1 to 4)

λ parameter defined by Eq. (34)

μ fluid viscosity (kg/m.s)

$\nu_{i\ell}$ stoichiometric coefficient for species i in reaction ℓ

ν_∞ bulk kinematic viscosity (m^2/s)

ρ	fluid density (kg/m^3)
σ	collision diameter for Lennard-Jones potential (m)
$\underline{\underline{\tau}}$	viscous stress tensor (N/m^2)
Ω	rotation speed of disk (rad/s)
Ω_s	shape parameter (rad/s)

Superscripts

*	ideal gas
-	partial molar quantity
T	transpose

Subscripts

ℓ	reaction ℓ
s	at surface
∞	in bulk

Table 1. Equilibrium Constants for Silicon Deposition Reactions; Coefficients for Equation (32).

	α_ℓ	β_ℓ	γ_ℓ
K_1	16.2412	-6730.9	-1.7004
K_2 (atm)	14.9848	-30520.7	0.5032
K_3	-1.0685	2229.3	-0.1756

Table 2. Values for Parameters in Equations (40) and (46)

Species, i	$\mu_i\,(Ns/m^2)$		$k_i\,(W/m.K)$	
	$10^7\delta_{1i}$	ψ_{1i}	δ_{2i}	ψ_{2i}
H_2	2.05	0.66	2.64×10^{-3}	0.725
HCl	1.06	0.87	7.36×10^{-5}	0.941
$SiCl_4$	0.75	0.87	4.10×10^{-5}	0.900
$SiHCl_3$	0.70	0.87	1.30×10^{-5}	1.070
$SiCl_2$	1.20	0.82	4.10×10^{-5}	0.900

Table 3. Values for Parameters in Equation (43) for Diffusion Coefficients

Species i	Species j	B_{ij}	ℓ_{ij}
H_2	HCl	4.376×10^{-7}	0.732
H_2	$SiCl_4$	2.190×10^{-7}	0.732
H_2	$SiHCl_3$	2.263×10^{-7}	0.732
H_2	$SiCl_2$	3.117×10^{-7}	0.714
HCl	$SiCl_4$	1.523×10^{-8}	0.873
HCl	$SiHCl_3$	1.601×10^{-8}	0.873
HCl	$SiCl_2$	2.491×10^{-8}	0.845
$SiCl_4$	$SiHCl_3$	6.109×10^{-9}	0.873
$SiCl_4$	$SiCl_2$	9.704×10^{-9}	0.845
$SiHCl_3$	$SiCl_2$	1.039×10^{-8}	0.845

Table 4. Values for Parameters in Equation (44) for Heat Capacities (J/mol.K)

Species, i	α_ℓ	β_ℓ	γ_ℓ
H_2	29.086	-8.110×10^{-4}	1.970×10^{-6}
HCl	28.219	1.756×10^{-3}	1.543×10^{-6}
$SiCl_4$	81.626	4.346×10^{-2}	-1.817×10^{-5}
$SiHCl_3$	61.035	6.477×10^{-2}	-2.472×10^{-5}
$SiCl_2$	48.056	1.684×10^{-2}	-7.084×10^{-5}

This report was done with support from the Department of Energy. Any conclusions or opinions expressed in this report represent solely those of the author(s) and not necessarily those of The Regents of the University of California, the Lawrence Berkeley Laboratory or the Department of Energy.

Reference to a company or product name does not imply approval or recommendation of the product by the University of California or the U.S. Department of Energy to the exclusion of others that may be suitable.

TECHNICAL INFORMATION DEPARTMENT
LAWRENCE BERKELEY LABORATORY
UNIVERSITY OF CALIFORNIA
BERKELEY, CALIFORNIA 94720